SCIENCE CHINA
Technological Sciences

• Article •

April 2023 Vol. 66 No. 4: 1050–1061
https://doi.org/10.1007/s11431-022-2102-3

Numerical and experimental studies on unsupervised deep Lagrangian learning based rotor balancing method

ZHONG Shun[1] & HOU Lei[2*]

[1]*Department of Mechanics, Tianjin University, Tianjin 300000, China;*
[2]*School of Astronautics, Harbin Institute of Technology, Harbin 150001, China*

Received May 16, 2022; accepted May 31, 2022; published online March 21, 2023

Rotor balancing is essential to rotor dynamic analysis. To make the balancing process convenient and costless, a balancing method using unsupervised deep Lagrangian network without weight trail is proposed. In the proposed network, a Lagrangian layer is applied to the network to introduce the physical prior knowledge. Compared to traditional balancing method, trail weight process is not necessary. Meanwhile, parameter sharing mechanics in baseline design or Lagrangian layer are applied to identify the unbalanced force without labeled data. Both numerical case study and corresponding experiment are conducted to validate the method. Both experimental and numerical results find that the proposed rotor balancing approach gives reasonable and comparative results with the considerations of both cost and accuracy. Compared with the baseline, to which no physical prior is applied, the balancing method with Lagrangian mechanism involved could achieve better performance. This proposed rotor dynamic balancing method gives out an alternative approach of rotor balancing methods.

rotor balancing, unsupervised deep learning, Lagrangian layer, weight trial, experimental rig, balancing experiment

Citation: Zhong S, HOU L. Numerical and experimental studies on unsupervised deep Lagrangian learning based rotor balancing method. Sci China Tech Sci, 2023, 66: 1050–1061, https://doi.org/10.1007/s11431-022-2102-3

1 Introduction

As the imbalance mass distribution is inevitable, the imbalance introduced vibration always observed in rotating machinery. The vibration usually leads to catastrophic failure [1,2]. To suppress the vibration amplitude, balancing process is conducted before the implementation. Especially, all rotors will experience factory balancing [3], on-site balancing [4] and online balancing [5]. Cost and accuracy are considered as key points in the overall evaluation of rotor dynamic balancing method. The modal balancing method (MBM) [6, 7] and the influence coefficient method (ICM) [8, 9] are usually adopted in industrial applications. Both of them have advantages and disadvantages, which are described in ref. [10].

To achieve better balancing performance, rotor dynamic balancing methods have been developed in recent years from variety of aspects. Untaroiu et al. [11] solved the influence coefficient balancing equations, which were considered with constraints of the residual vibrations and correction weights in inequality forms by the numerical algorithms developed in convex optimization theory to identify the suitable trail weights. Wang [12] formulated the flexible rotor balancing problem based on the influence coefficient method with holo-spectrum technique as a mini-max optimisation problem. Messager and Pyrz [13] dealt with the optimization problem of the rotor balancing by two-plane dynamical balancing. Kang et al. [14] simulated the flexible rotor dynamical balancing problem by finite element method to simulate the flexibility of balancing. In their work, various sensors and planes are arranged to achieve better performance. Li et al. [15] considered the high-speed flexible rotor balancing as an optimization problem and solved it by optimiza-

*Corresponding author (email: houlei@hit.edu.cn)

tion theory. Zhang et al. [16, 17] identified imbalance of a dual-rotor system by correlation methods with whole beat or non-whole beat. Tresser et al. [18] proposed a balancing method which could balance the rotor with high-speed working conditions only by its low-speed signals. Khulief et al. [19] combined two classical balancing methods of the influence coefficient method and modal balancing techniques to balance the flexible rotor. Deepthikumar et al. [20] used finite element modeling method to establish the rotor model and a polynomial curve of eccentricity distribution to identify the imbalance. Villafane Saldarriaga et al. [21] proposed a methodology which used experiment results to identify a matrix relating unbalance forces to measured displacements. Han [22] gave out a new generalized modal balancing method for non-isotropic rotors.

With the help of the finite element simulation, Li et al. [23] proposed a novel modal balancing technique which could calculate the trail weight numerically. Thus, their balancing methods did not need trial weight process any more. Yue et al. [24] investigated on the complex structure rotor. In their studies, the residual imbalance from different correction planes was estimated and the effects were compared. With the help of the transient responses of the rotor system, Zhao et al. [10] proposed a novel balancing method with only transient signals. Li et al. [25] proposed a field dynamical balancing method with the help of disturbance observers. Zheng and Wang [26] presented a high-precision field dynamical balancing method by regular control.

Meanwhile, deep learning technologies have developed fast in recent years and have been applied to many enginering fields [27, 28]. One of their applications is to tackle input identification problems by learning a inverse mapping function by measured data [29–33]. To the rotor balancing problem, the training of the inverse function could be conducted from the same data usually used for normal balancing process. For example, Zhang et al. [34, 35] investigated the rotor dynamics and fault diagnosis of the rotor system successfully by deep learning technologies. Ding et al. [36] monitored the bearing working conditions of an aero-engine by sparsity-assisted intelligence. Then same group proposed an interpretable fault diagnosis deep network which could be against noise attack [37]. Thus, we try to establish a deep neutral network based on balancing method with deep-learning technologies.

The rest of the our work is organized as follows. In Sect. 2, the fundamental of the prime originality of the proposed method is introduced. Sect. 3 shows the proposed network in detail. Numerical validation and experimental validation are undertaken in Sects. 4 and 5 separately. The paper is concluded finally.

2 Preliminary-Lagrangian network

In dynamics theories, a mapping function f can be used either to predict the evolution of the state variables in forward way or identify the input τ by its inverse form f^{-1},

$$\begin{aligned} &f(\boldsymbol{q}, \dot{\boldsymbol{q}}, \boldsymbol{\tau}) = \ddot{\boldsymbol{q}}, \\ &f^{-1}(\boldsymbol{q}, \dot{\boldsymbol{q}}, \ddot{\boldsymbol{q}}) = \boldsymbol{\tau}, \end{aligned} \tag{1}$$

where $\boldsymbol{q}$ is the generalized coordinate displacement vector. $\dot{\boldsymbol{q}}$ and $\ddot{\boldsymbol{q}}$ are corresponding generalized velocity and acceleration vectors. Various formalism that could derive the equations described by eq. (1) has been developed. The most prominent are Newtonian-, Hamiltonian-, and Lagrangian-mechanics [38].

When Lagrangian-mechanics is applied, choosing Lagrangian function L_f to be

$$L_f = T_f - V_f, \tag{2}$$

where T_f refers to the kinetic energy of the system represented by mapping function f and V_f the corresponding potential energy of the same system. Based on the Lagrangian theory, the Euler-Lagrange equation with non-conservative forces can be obtained.

$$\frac{\mathrm{d}}{\mathrm{d}t}\frac{\partial L_f}{\partial \dot{\boldsymbol{q}}_i} - \frac{\partial L_f}{\partial \boldsymbol{q}_i} = \boldsymbol{\tau}, \tag{3}$$

where τ is the general force.

The kinetic energy T_f could be computed by generalized coordinates as $T_f = 1/2 \cdot \dot{\boldsymbol{q}}^{\mathrm{T}} \cdot \boldsymbol{H}(\boldsymbol{q}) \cdot \dot{\boldsymbol{q}}$, where $\boldsymbol{H}(\boldsymbol{q})$ represents general mass matrix. Substituting eq. (2) into eq. (3) yields

$$\boldsymbol{H}(\boldsymbol{q}) \cdot \ddot{\boldsymbol{q}} + \dot{\boldsymbol{H}}(\boldsymbol{q}) \cdot \dot{\boldsymbol{q}} - \frac{1}{2} \cdot \left(\frac{\partial}{\partial \boldsymbol{q}} (\dot{\boldsymbol{q}}^{\mathrm{T}} \cdot \boldsymbol{H}(\boldsymbol{q}) \cdot \dot{\boldsymbol{q}}) \right)^{\mathrm{T}} + \frac{\mathrm{d}V}{\mathrm{d}\boldsymbol{q}} = \boldsymbol{\tau}. \tag{4}$$

Further, a lower triangular matrix $\boldsymbol{L}(\boldsymbol{q})$ can be used to represent $\boldsymbol{H}(\boldsymbol{q}) = \boldsymbol{L}(\boldsymbol{q}) \cdot \boldsymbol{L}(\boldsymbol{q})^{\mathrm{T}}$ to ensure the positive definiteness of $\boldsymbol{H}(\boldsymbol{q})$.

3 Proposal of the method

3.1 Deep Lagrangian network for rotor balancing

Starting from eq. (1), if neutral networks are applied to the mechanical system, the forward mapping and inverse mapping can be learned by measured or observed data,

$$\begin{aligned} &\hat{f} = \hat{f}(\boldsymbol{q}, \dot{\boldsymbol{q}}, \boldsymbol{\tau}; \boldsymbol{\alpha}), \\ &\hat{f}^{-1} = \hat{f}^{-1}(\boldsymbol{q}, \dot{\boldsymbol{q}}, \ddot{\boldsymbol{q}}; \boldsymbol{\beta}), \end{aligned} \tag{5}$$

where $\boldsymbol{\alpha}$ and $\boldsymbol{\beta}$ refer to the trainable variables of the mapping function. The network learns the inverse mapping f^{-1} from generalized coordinate displacement, velocity and acceleration $(\boldsymbol{q}, \dot{\boldsymbol{q}}, \ddot{\boldsymbol{q}})$ to the general force $\boldsymbol{\tau}$. More in detail, the

trainable parameters are updated by minimizing the errors between the real values of $(\boldsymbol{q}, \dot{\boldsymbol{q}}, \ddot{\boldsymbol{q}}, \boldsymbol{\tau})$ and the predicted values.

To the rotor balancing problem, our aim is to identify the general forces through the measured state variables, such as displacements and velocities. These data can be measured by enlarging the sample frequency or sample time in one test run of the rotor. In other words, only by one run of the rotor system, enough data for identification problem can be obtained, by which the network can be trained and then predicts the trail weight. Thus, in the proposed method, no more weight trail process is needed.

The baseline to solve this problem is training the trainable parameters by minimizing the ℓ_i norm of the predictions of eq. (1) and measured force $\boldsymbol{\tau}$.

$$\boldsymbol{\beta}^* = \arg\min_{\boldsymbol{\beta}} \ell_i(\hat{f}^{-1}(\boldsymbol{q}, \dot{\boldsymbol{q}}, \ddot{\boldsymbol{q}}; \boldsymbol{\beta}), \boldsymbol{\tau}). \tag{6}$$

Further, considering the basic physical knowledge and improving the performance, an additional layer of Lagrangian can be applied, whose structure is given in Figure 1.

As Figure 1(a) illustrates, the joint configurations are used to train layers of the basic network (BN). Then the Lagrangian layer adds physical prior knowledge to the whole network and gets the output tensor of general forces. The basic network, whose structure is given in Figure 1(b) and described by

$$\begin{aligned}
&\boldsymbol{a}_i = \boldsymbol{W}_i \cdot \boldsymbol{h}_{i-1} + \boldsymbol{b}_i,\\
&\boldsymbol{h}_i = g_i(\boldsymbol{a}_i),\\
&\frac{\partial \boldsymbol{h}_i}{\partial \boldsymbol{h}_{i-1}} = \mathrm{diag}(g_i'(\boldsymbol{a}_i)) \cdot \boldsymbol{W}_i,
\end{aligned}$$

computes $\boldsymbol{L}(\boldsymbol{q})$ and $\frac{\partial \boldsymbol{L}}{\partial \boldsymbol{q}}$ simultaneously and analytically by applying the chain rule of

$$\frac{\partial \boldsymbol{L}}{\partial \boldsymbol{q}} = \frac{\partial \boldsymbol{L}}{\partial \boldsymbol{h}_{i-1}} \cdot \frac{\partial \boldsymbol{h}_i}{\partial \boldsymbol{h}_{i-2}} \cdots \frac{\partial \boldsymbol{h}_1}{\partial \boldsymbol{q}}. \tag{7}$$

With the introduction of the Lagrangian layer, $\boldsymbol{L}(\boldsymbol{q})$ and $V(\boldsymbol{q})$ are represented by the network instead of the general forces. Therefore, the estimations of $\boldsymbol{L}(\boldsymbol{q})$ and $V_f(\boldsymbol{q})$ are

$$\begin{aligned}
&\hat{\boldsymbol{L}}(\boldsymbol{q}) = \hat{\boldsymbol{L}}(\boldsymbol{q}; \boldsymbol{\theta}),\\
&\hat{V}(\boldsymbol{q}) = \hat{V}(\boldsymbol{q}; \boldsymbol{\psi}),
\end{aligned}$$

and the optimization problem is described by

$$(\boldsymbol{\theta}^*, \boldsymbol{\psi}^*) = \arg\min_{\boldsymbol{\theta}, \boldsymbol{\psi}} \ell_i(\hat{f}^{-1}(\boldsymbol{q}, \dot{\boldsymbol{q}}, \ddot{\boldsymbol{q}}; \boldsymbol{\theta}, \boldsymbol{\psi}), \boldsymbol{\tau}) \tag{8}$$

with

$$\begin{aligned}
\hat{f}^{-1}(\boldsymbol{q}, \dot{\boldsymbol{q}}, \ddot{\boldsymbol{q}}; \boldsymbol{\theta}, \boldsymbol{\psi}) =& \hat{H}(\boldsymbol{q}) \cdot \ddot{\boldsymbol{q}} + \frac{\mathrm{d}}{\mathrm{d}t} \hat{\boldsymbol{H}}(\boldsymbol{q}) \cdot \dot{\boldsymbol{q}}\\
&- \frac{1}{2} \cdot \left(\frac{\partial}{\partial \boldsymbol{q}} (\dot{\boldsymbol{q}}^{\mathrm{T}} \cdot \hat{\boldsymbol{H}}(\boldsymbol{q}) \cdot \dot{\boldsymbol{q}}) \right)^{\mathrm{T}} + \frac{\mathrm{d}\hat{V}}{\mathrm{d}\boldsymbol{q}}.
\end{aligned}$$

3.2 Introducing of the forward model

Another benefit to introduce the Lagrangian layer is that one can combine the forward model loss to the inverse model loss. Because only $\boldsymbol{L}(\boldsymbol{q})$ and $V_f(\boldsymbol{q})$ are represented by the networks, the forward model can be constructed by Lagrangian equation as

$$\hat{\boldsymbol{H}}^{-1}(\boldsymbol{q}) \cdot \left[\boldsymbol{\tau} - \frac{\mathrm{d}}{\mathrm{d}t} \hat{\boldsymbol{H}}(\boldsymbol{q}) \cdot \boldsymbol{q} + \frac{1}{2} \left(\frac{\partial}{\partial \boldsymbol{q}} (\dot{\boldsymbol{q}}^{\mathrm{T}} \cdot \hat{\boldsymbol{H}}(\boldsymbol{q}) \cdot \hat{\boldsymbol{q}}) \right) \right]^{\mathrm{T}} - \frac{\partial \hat{V}}{\partial \boldsymbol{q}} = \ddot{\boldsymbol{q}}. \tag{9}$$

When introducing the forward loss, the combination loss function can be structured, e.g.,

$$\begin{aligned}
(\boldsymbol{\theta}^*, \boldsymbol{\psi}^*) = \arg\min_{\boldsymbol{\theta}, \boldsymbol{\psi}} &(\ell_i(\hat{f}^{-1}(\boldsymbol{q}, \dot{\boldsymbol{q}}, \ddot{\boldsymbol{q}}; \boldsymbol{\theta}, \boldsymbol{\psi}), \boldsymbol{\tau})\\
&+ \ell_i(\hat{f}(\boldsymbol{q}, \dot{\boldsymbol{q}}, \boldsymbol{\tau}; \boldsymbol{\theta}, \boldsymbol{\psi}), \ddot{\boldsymbol{q}})).
\end{aligned} \tag{10}$$

3.3 Unsupervised mechanism for unbalanced force

If the unbalanced forces were learned supervisedly, several runs of a standard rotor system with pre-set imbalance distributions have to be undertaken. However, it is not a good choice to do so, considering the cost and condition. Therefore, in this section, an unsupervised mechanism for unbalanced force is introduced in the whole network to learn the inverse mapping without labeled unbalanced forces.

In rotor balancing problem, the general force mainly includes two parts. One is the unbalanced force and the other is the bearing force. If we could measure these forces, the measured forces can be used as label data to help in training the network. Unfortunately, the unbalanced force could not be measured. At the same time, the bearing forces are not easy to measure either. But, the bearing forces can be estimated indirectly through the Newton law.

$$\boldsymbol{\tau}_{sm_i} = m_i a_i - F_i, \tag{11}$$

where m_i refers to the equivalent mass of the support structure. a_i is the acceleration of the support and F_i the corresponding force got by dynamical force sensor. So supports' information is necessary for this proposed method. Based on these, the whole scheme for baseline is shown in Figure 2.

In real practise, eddy current sensors are always used to measure the vibration of the shaft at certain points. Thus, in order to get corresponding velocity and acceleration, a preprocessing module is applied to the whole network to derive the measured displacement in Figure 2. The neutral network module could have arbitrary type, only increasing the complexity of the network and changing the shape of the data set. The three 1-dimensional convolutional layers are applied to separate bearing force vector $\boldsymbol{\tau}_s$ with unbalanced force vector $\boldsymbol{\tau}_u$. In this way, $\boldsymbol{\tau}_s$ is involved in training process as it

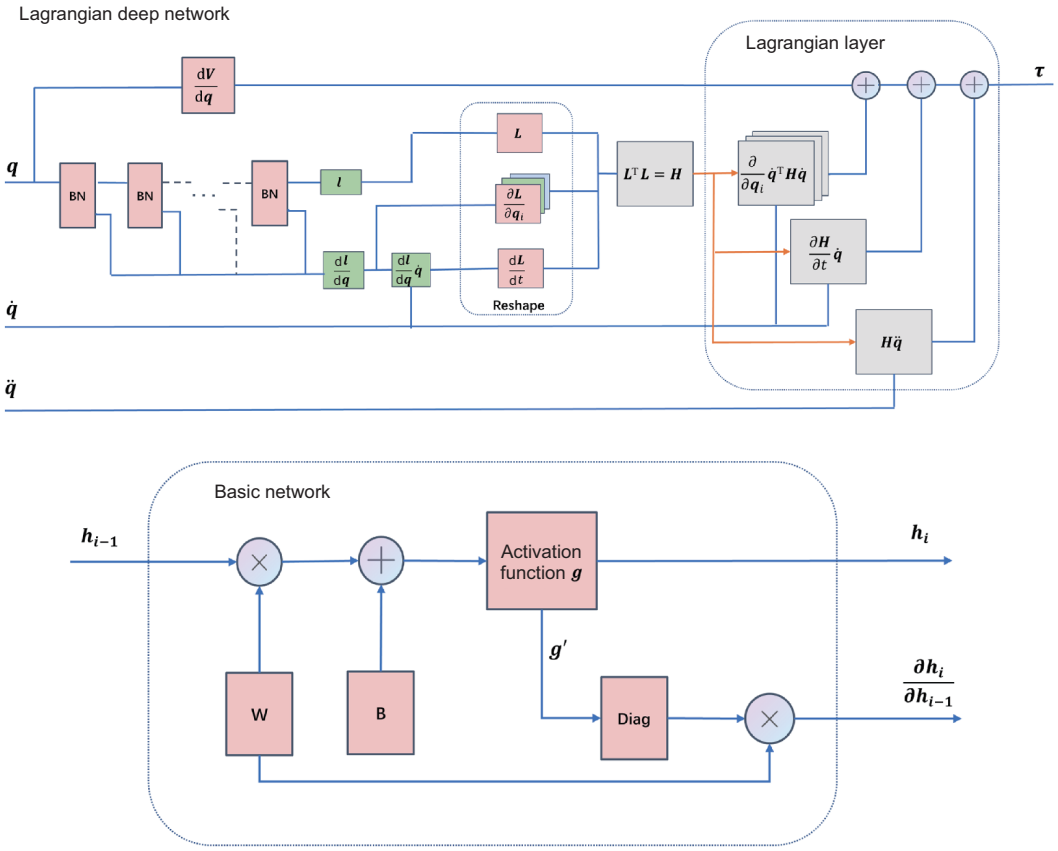

Figure 1 (Color online) The overview of the Lagrangian deep network (LDN). (a) The structure of whole LDN and (b) the structure of basic network (BN).

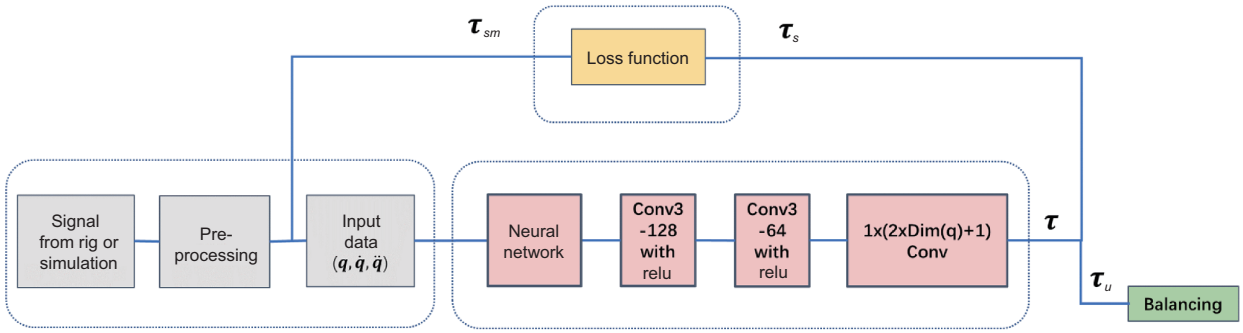

Figure 2 (Color online) The overview of the unsupervised network in baseline design, where Conv"X"-"N" refers to a convolutional layer having "N" filters with size of $1 \times$ "X".

is used to solve the optimization problem described by slight modification of eq. (6) to

$$\boldsymbol{\beta}^* = \arg\min_{\boldsymbol{\beta}} L((\hat{f}^{-1}(\mathbf{q}, \dot{\mathbf{q}}, \ddot{\mathbf{q}}; \boldsymbol{\beta}))_s, \boldsymbol{\tau}_{sm}), \tag{12}$$

where L is an arbitrary type loss function, say, mean square error. $\boldsymbol{\tau}_u$ is considered to be the prediction of the unbalanced force. In other words, $\boldsymbol{\tau}_u$ is learned unsupervisedly. This structure are described in detail in ref. [39].

When LDN is applied, the whole scheme can be changed into Figure 3. In Figure 3, the LDN module changes the data shape from three times dimension of the general displacements to two times number of the state variables. With the introduction of the Lagrangian layer, no additional convolutionals are needed to separate the bearing force $\boldsymbol{\tau}_s$ and the immeasurable unbalanced force $\boldsymbol{\tau}_u$. Following the same rule of the baseline, $\boldsymbol{\tau}_s$ is involved in the optimization problem, and $\boldsymbol{\tau}_u$ refers to the unbalanced force. All the trainable parameters of the network are updated by back propagation mechanism. Then the inverse mapping f^{-1} is learned.

In this scheme, the optimization problem is described by a

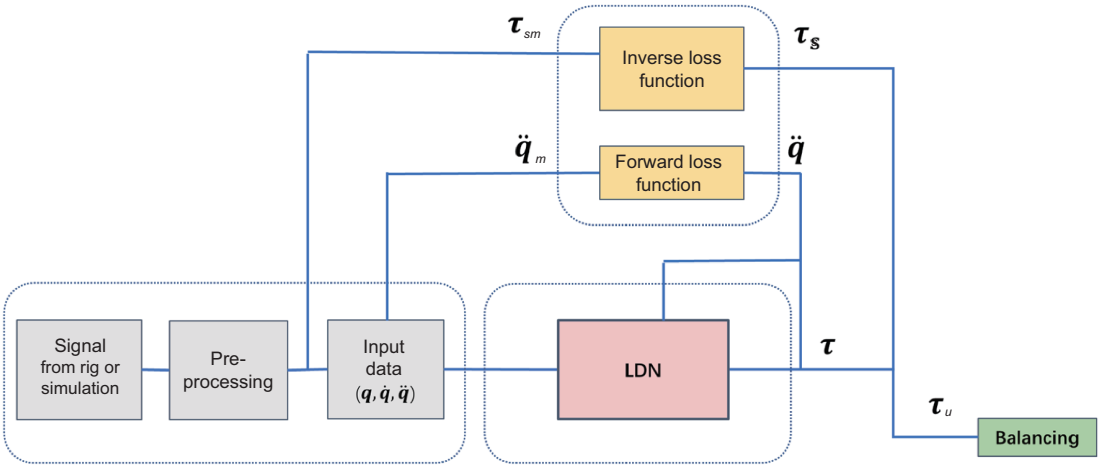

Figure 3 (Color online) Overview of the unsupervised network with the application of the Lagrangian layer.

modification of eq. (8) to

$$(\boldsymbol{\theta}^*, \boldsymbol{\psi}^*) = \arg\min_{\boldsymbol{\theta},\boldsymbol{\psi}} \ell_i(\hat{f}^{-1}(\boldsymbol{q}, \dot{\boldsymbol{q}}, \ddot{\boldsymbol{q}}; \boldsymbol{\theta}, \boldsymbol{\psi})_s, \boldsymbol{\tau}_{sm}) \tag{13}$$

without forward loss or eq. (10) to

$$\begin{aligned}(\boldsymbol{\theta}^*, \boldsymbol{\psi}^*) =& \arg\min_{\boldsymbol{\theta},\boldsymbol{\psi}} (\ell_i(\hat{f}^{-1}(\boldsymbol{q}, \dot{\boldsymbol{q}}, \ddot{\boldsymbol{q}}; \boldsymbol{\theta}, \boldsymbol{\psi})_s, \boldsymbol{\tau}_{sm}) \\ &+ \ell_i(\hat{f}(\boldsymbol{q}, \dot{\boldsymbol{q}}, \hat{\boldsymbol{\tau}}; \boldsymbol{\theta}, \boldsymbol{\psi}), \ddot{\boldsymbol{q}}))\end{aligned} \tag{14}$$

with forward loss involved.

4 Numerical validation

4.1 Modeling

In numerical study, a four discs rotor with pre-set imbalance model is adopted to validate the proposed approach in numerical way. Figure 4 gives out the schematic graph of the rotor, which consists of four discs and two ball bearings.

Considering gyroscopic effect and general forces, the governing equations of the rotor structure described in Figure 4 is established by following the Newton law.

$$\boldsymbol{M} \cdot \ddot{\boldsymbol{q}} + (\boldsymbol{C} + \Omega \cdot \boldsymbol{G}) \cdot \dot{\boldsymbol{q}} + \boldsymbol{K} \cdot \boldsymbol{q} + \boldsymbol{F}_n = \boldsymbol{F}_u + \boldsymbol{F}_g, \tag{15}$$

where $\boldsymbol{q}$ refers to the displacement coordinate vector, including the displacements of four discs, which are numbered from (#2 to #5) and two ball bearings, which are numbered as #1 and #6 along the x-axis and y-axis, respectively. $\boldsymbol{M}$, $\boldsymbol{C}$, $\boldsymbol{G}$ and $\boldsymbol{K}$ are corresponding mass, damping, gyro and stiffness matrices. $\boldsymbol{F}_n$ refers to the bearing force, $\boldsymbol{F}_u$ refers to the unbalanced force and $\boldsymbol{F}_g$ gravity. Ω is the rotating speed.

In numerical simulation, the deep groove bearing force model is adopted [40]. In the model, the bearing force of the right end is

$$\begin{bmatrix} F_{bx1} \\ F_{by1} \end{bmatrix} = C_b \sum_{i=1}^{N_b} (\delta_{1i} H[\delta_{1i}])^{3/2} \begin{bmatrix} \cos\theta_{1i} \\ \sin\theta_{1i} \end{bmatrix}, \tag{16}$$

where $\delta_{1i} = x_1 \cos\theta_i + y_1 \sin\theta_i - \delta_0$. θ_i is the position of i-th ball. C_b is the Hertz contact stiffness. $H[\cdot]$ is Heaviside function and δ_0 is the radial clearance.

Accordingly, the left end force can be expressed as

$$\begin{bmatrix} F_{bx2} \\ F_{by2} \end{bmatrix} = C_b \sum_{i=1}^{N_b} (\delta_{2i} H[\delta_{2i}])^{3/2} \begin{bmatrix} \cos\theta_{2i} \\ \sin\theta_{2i}, \end{bmatrix}, \tag{17}$$

where $\delta_{2i} = x_6 \cos\theta_i + y_6 \sin\theta_i - \delta_0$.

Figures 5–7 give the responses of the vertical responses, horizontal responses and forces of the numerical simulation results of the system described by eq. (15). These data will be then used as training data to train the proposed network in numerical sense.

4.2 Identification of the trail weight and response prediction of the system

In numerical validation, the training dataset is the simulation responses of the rotor model described by eq. (15). The eq. (15) is integrated by Runge-Kutta method. In the calculation, the initial values are zeros. The responses of the state variables which include displacement and velocity are got by directly integration, while the accelerations are got by solving the eq. (15) algebraically.

The simulation time span is 20 s, with time interval of 0.001 s. The length of the data set is fixed to 20000. In this example, the length of sample is set to 1. Inputting the joint configurations $(q, \dot{q}, \ddot{q})$, by optimizing the loss function of the τ_s-dimensional outputs and the measured τ_{sm}, the trainable parameters can be updated. Adam optimizer, mean square error of τ_{sm} and τ_s and mini-batch of 128 are applied.

The predictions of the unbalanced forces are given in Figure 8. The corresponding identification results are listed in

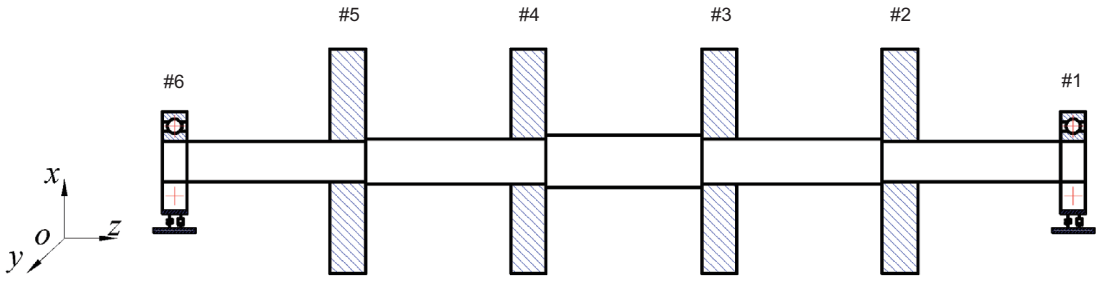

Figure 4 (Color online) Schematic diagram of the rotor.

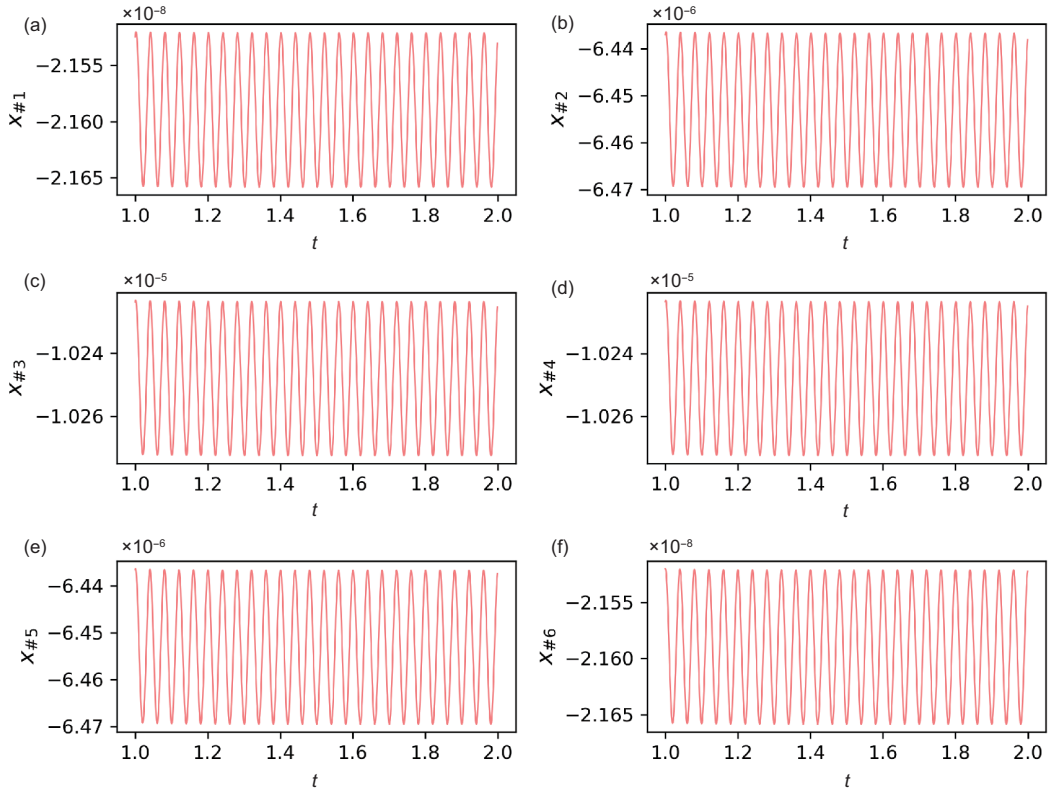

Figure 5 (Color online) Vertical responses of (a) node 1, (b) node 2, (c) node 3, (d) node 4, (e) node 5 and (f) node 6.

Table 1. The pre-set values are randomly chosen in this simulation, which are also listed in Table 1.

Based on the identification results listed in Table 1, the rotor system with pre-set imbalance is balanced. The balancing results are shown in Figures 9 and 10. In Figure 9, the red lines give the responses of nodes of #1 to #6 in vertical direction with pre-set imbalance. The black broken lines are the response curves when the rotor is balanced by the identification value of imbalance listed in Table 1. Comparing the amplitudes of the responses curves before and after balancing, it is noting that the balancing effect is reasonable as the amplitudes of the responses reduce significantly. In Figure 10, the comparison results are given in horizontal direction. It can be found that the results in horizontal direction follow the same trends as those in vertical direction but with the balancing effects not as good as those in vertical direction.

Table 1 The identification results in numerical way

	Pre-set value	Identification value
Amplitude on correction plane one	1.1	1.0902
Phase on plane one	$\pi/2$	1.8236
Amplitude on correction plane two	1.1	1.1037
Phase on plane two	$\pi/3$	1.3392

5 Experimental analysis

5.1 Set up of experimental rig

In order to study this problem in practical way, an experi-

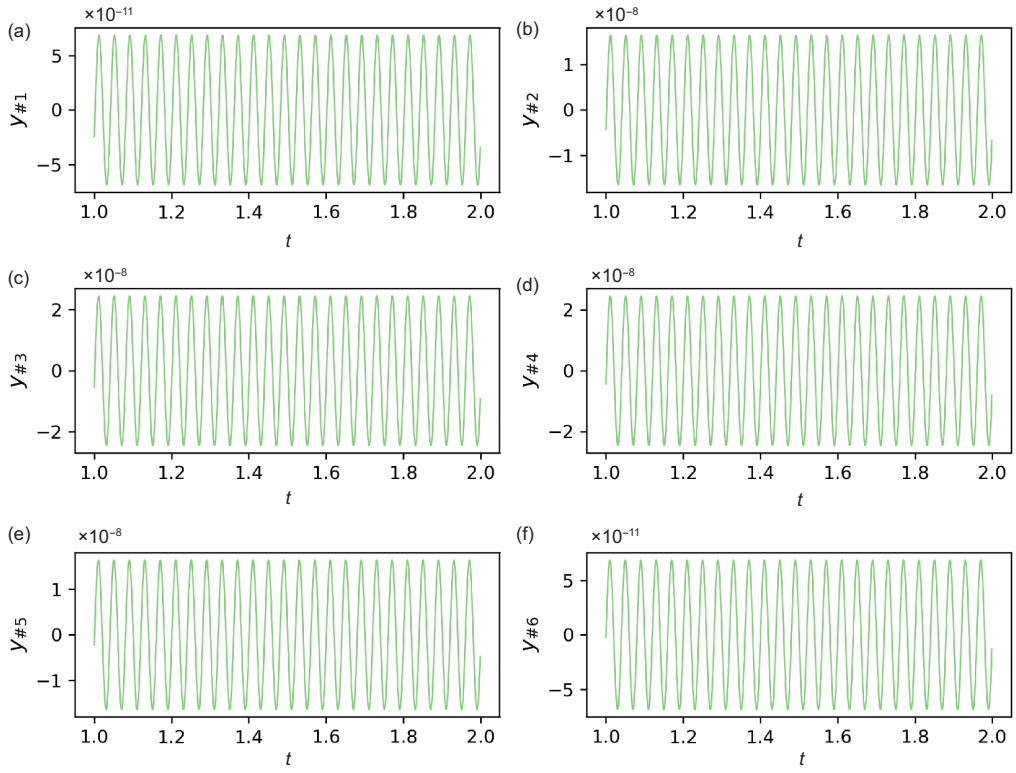

Figure 6 (Color online) Horizontal responses of (a) node 1, (b) node 2, (c) node 3, (d) node 4, (e) node 5 and (f) node 6.

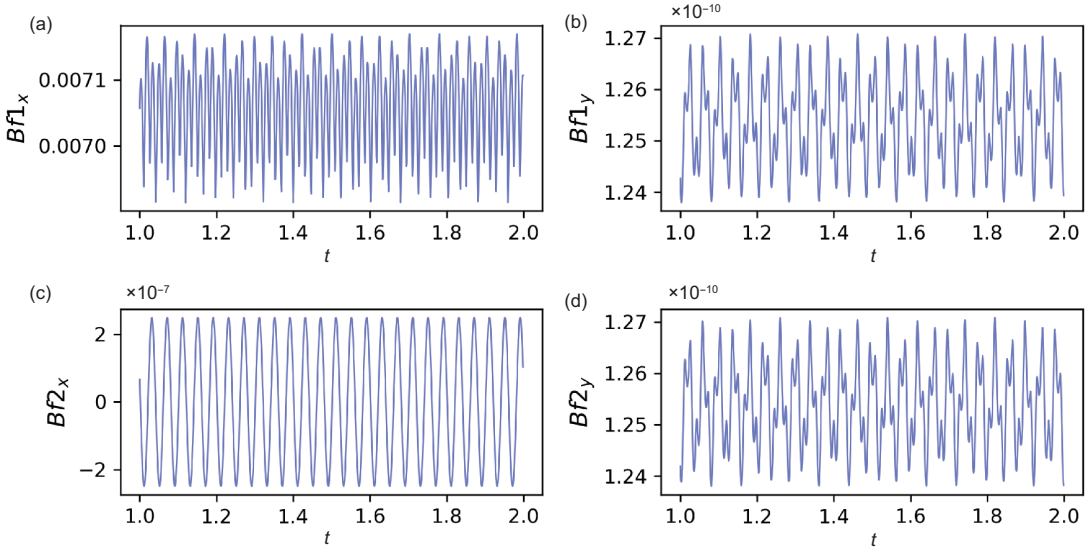

Figure 7 (Color online) Forces of (a) bearing 1 in vertical direction, (b) bearing 1 in horizontal direction, (c) bearing 2 in vertical direction and (d) bearing 2 in horizontal direction.

mental rig is established. The overview of the set up rig is sketched in Figure 11. The rotor rig is composed of a rotor base, a speed-regulating motor, two bearing supports, an elastic coupling, a rotor shaft, four rotor discs, six eddy current sensors, two dynamic force sensors, a photoelectric test sensor and a signal amplification and a storage module. The fundamental part of the rig is a single rotor with four discs and two ball-bearing supports. The rotor is driven by a speed-regulating motor with maximum power of 148 W. The motor driver rectifies the 220 V AC power supply and outputs a PWM signal to drive the rotor. Connected with a elastic coupling, the rotor rotating speed can be adjusted from 0 to 2000 r/min. The rotor is supported by two ball bearings, which mounted elastically on the base. The distance between two

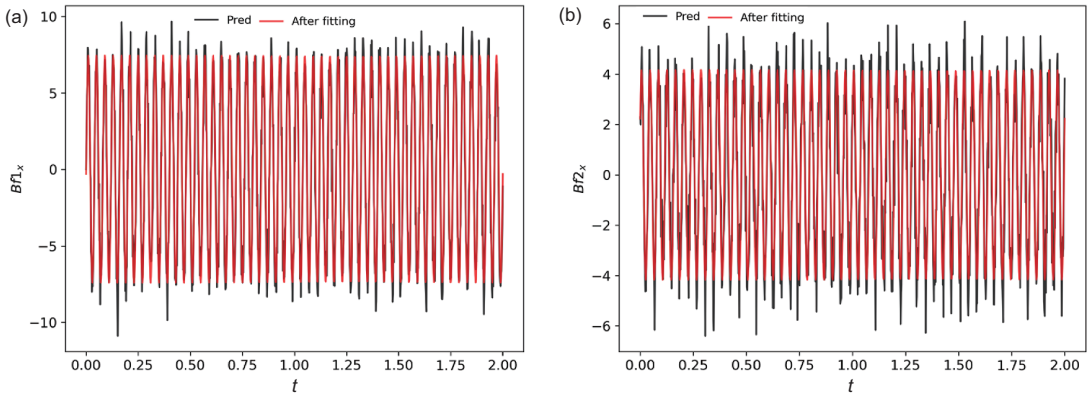

Figure 8 The predictions of the unbalanced forces and their identifications. (a) Correction plane 1 and (b) correction plane 2.

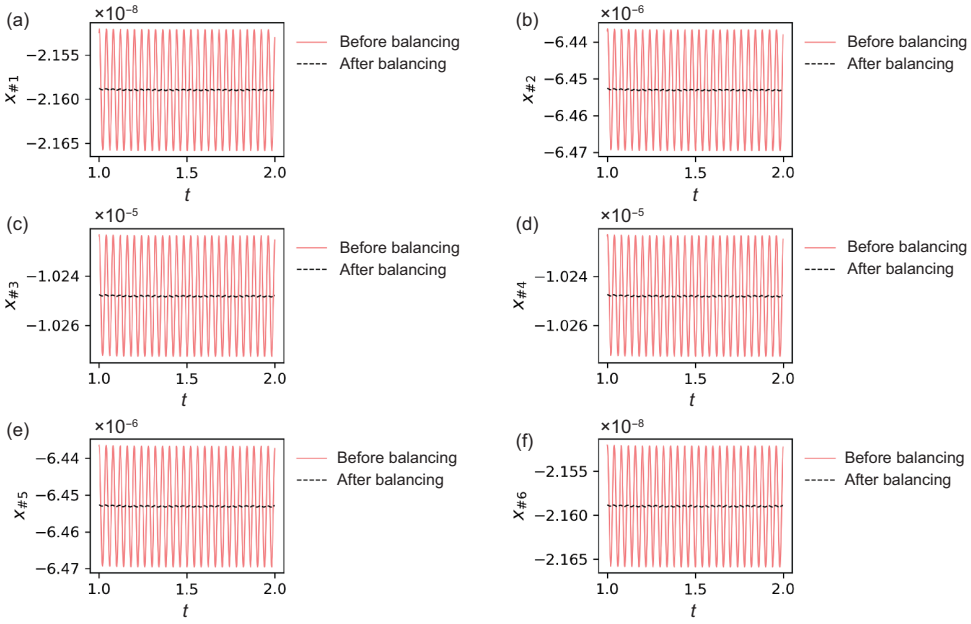

Figure 9 Balancing results of (a) node 1, (b) node 2, (c) node 3, (d) node 4, (e) node 5 and (f) node 6 in vertical direction.

bearings is 375 mm. Between them, four discs are installed equidistantly. Each disc has a diameter of 50 mm and a thickness of 16 mm. From right to left in front view of the rig (Figure 11(b)), two bearings and four discs are numbered by #1 to #6 successively.

Six eddy current sensors are installed near each numbered nodes separately through brackets to collect displacement signals of the horizontal vibration of the chosen nodes. Two dynamic force sensors are amounted at #1 node and #6 node to measure the forces, which will be used to estimate the horizontal components of bearing forces. A photoelectric sensor is installed on the side of the coupling through a bracket and a piece of reflective paper is attached to the coupling. The photoelectric sensor generates a pulse with the rotating frequency. This pulse signal serves as a reference for the rotating speed and initial vibration phase. A signal collection equipment with type of DH5922N is used to amplify, rectify and store the measured signals. The sampling frequency is set to 500 Hz. The sensors used to measure the data are shown in Figure 12.

5.2 Experimental data preparing

The frequency of vibration caused by imbalance distribution equals to the rotating speed. Thus, the raw measured responses need pre-processing before being used for balancing process. The working frequency is set to 1500 r/min. Thus, a band-pass filter from 5 to 30 Hz is applied to the measured response. Then the base frequency component is filtered for balancing.

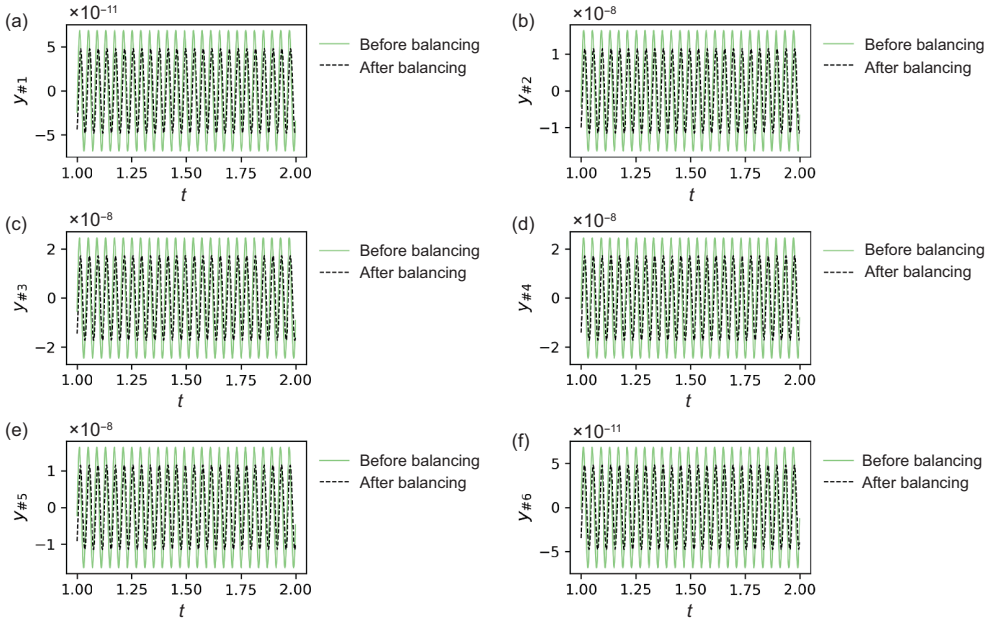

Figure 10 Balancing results of (a) node 1, (b) node 2, (c) node 3, (d) node 4, (e) node 5 and (f) node 6 in horizontal direction.

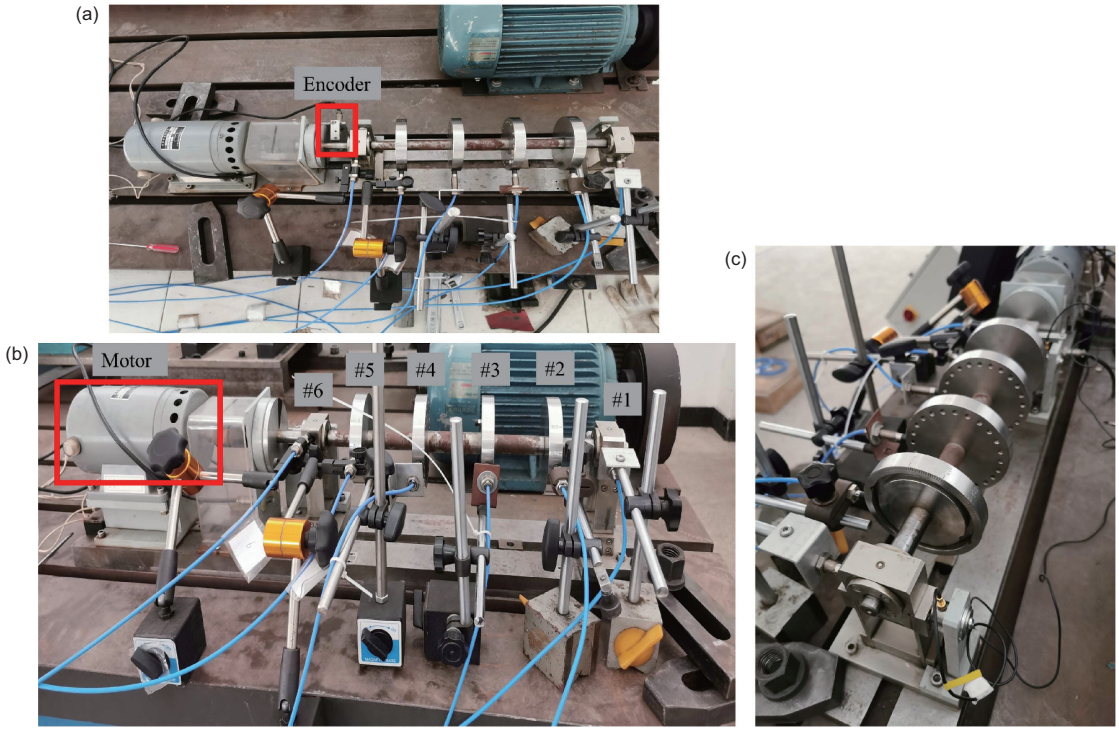

Figure 11 Overview of the experimental rig from (a) top direction, (b) front direction and (c) side directions.

5.3 Compared approach

In this subsection, two approaches are applied to identify the equivalent imbalance masses on selected correction planes. The first one is the baseline, i.e., only unsupervised mechanism is applied to the whole network and no Lagrangian layer is applied. For the second approach, the unsupervised deep learning balancing method is adopted. In both approaches, #2 and #5 discs are selected as correction planes. The radium of balancing groove is 40 mm on each disc.

For unsupervised deep learning method, not only the pre-processed raw signals measured from #1 to #6 nodes, but also

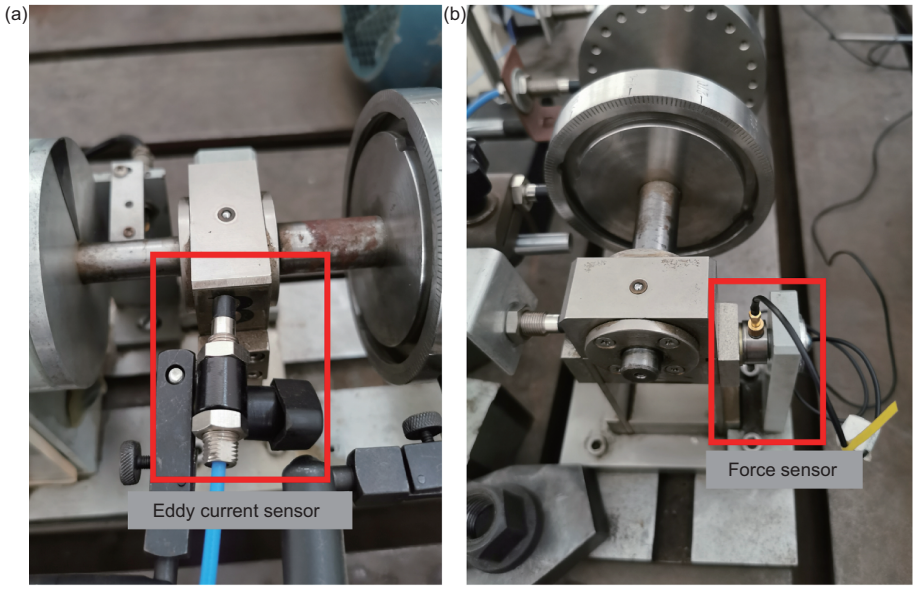

Figure 12 (Color online) Instruction of the sensors implemented in the experimental rig. (a) Eddy current sensor and (b) dynamic force sensor.

the forces measured by dynamic force sensors are used for training the network. The displacements are measured directly. The velocities and accelerations are got by deriving the displacement numerically. The bearing forces can be estimated by solving eq. (11) with the reference of measured force signals algebraically.

The raw data are collected within a time period of 15 s with sampling frequency of 500 Hz. The length of each sample is set to 1, which means the size of the training data is 7500. Then, the joint configurations $(\boldsymbol{q}, \dot{\boldsymbol{q}}, \ddot{\boldsymbol{q}})$ from the training dataset will be input to the network described in Figure 3(b). The joint optimization function described by eq. (14) is used for training process. The mean square error is adopted for calculating the loss. Meanwhile, mini-batch with size of 128 and Adam optimizer are applied in the training of the network. After 2000 epochs, the predictions of the unbalanced forces are fitted for balancing the rotor. The results by unsupervised deep learning (UDL) and unsupervised deep Lagrangian network (UDLN) are listed in Table 2.

With the identification results of the amplitudes and the phases of the unbalanced forces by UDL and UDLN, the experimental rotor structure can be balanced. The performance after balancing is illustrated by Figure 13. In Figure 13, light blue lines indicate the responses of unbalanced rotor system after pre-processing. The black broken lines give the responses of the balanced rotor after balancing by results from UDL. The red curves are the responses of the rotor balanced by UDLN. From the comparisons, we could find that both UDL and UDLN can balance the rotor and the amplitude of the the responses reduce significantly after balancing. With these two methods compared, the results by UDLN are better than UDL.

Table 2 The identification results of the imbalance mass distribution

	UDL	UDLN
Correction mass at plane 1	8.42 g	7.37 g
Correction phase at plane 1	285.2°	267.0°
Correction mass at plane 2	6.3 g	4.17 g
Correction phase plane 2	156.4°	303.3°

6 Conclusions

A deep Lagrangian learning based rotor dynamical balancing method is proposed in this work. With joint configurations of the general state variables and accelerations in just one run of the system, the proposed method balances the rotor structure. That means the proposed method realizes the balancing process without weight trails. A particular Lagrangian layer is applied to the architecture of the proposed network to introduce prior physical knowledge of the mechanical system to understand the essential better. Meanwhile, the unsupervised mechanism is introduced in the network to learn unbalanced force without the help of labeled data. Both the numerical and experimental studies are conducted to prove the validation of the proposed method. The balancing results of the simulation and experiment prove that the proposed method is reasonable and comparative (costless and better performance).

Meanwhile, it is worth noting that in the architecture of the proposed network, almost all parameters could be adjusted and optimized, which leaves us an optimization problem for further development of the balancing performance. And the sample data size can also be enlarged, so that more historic

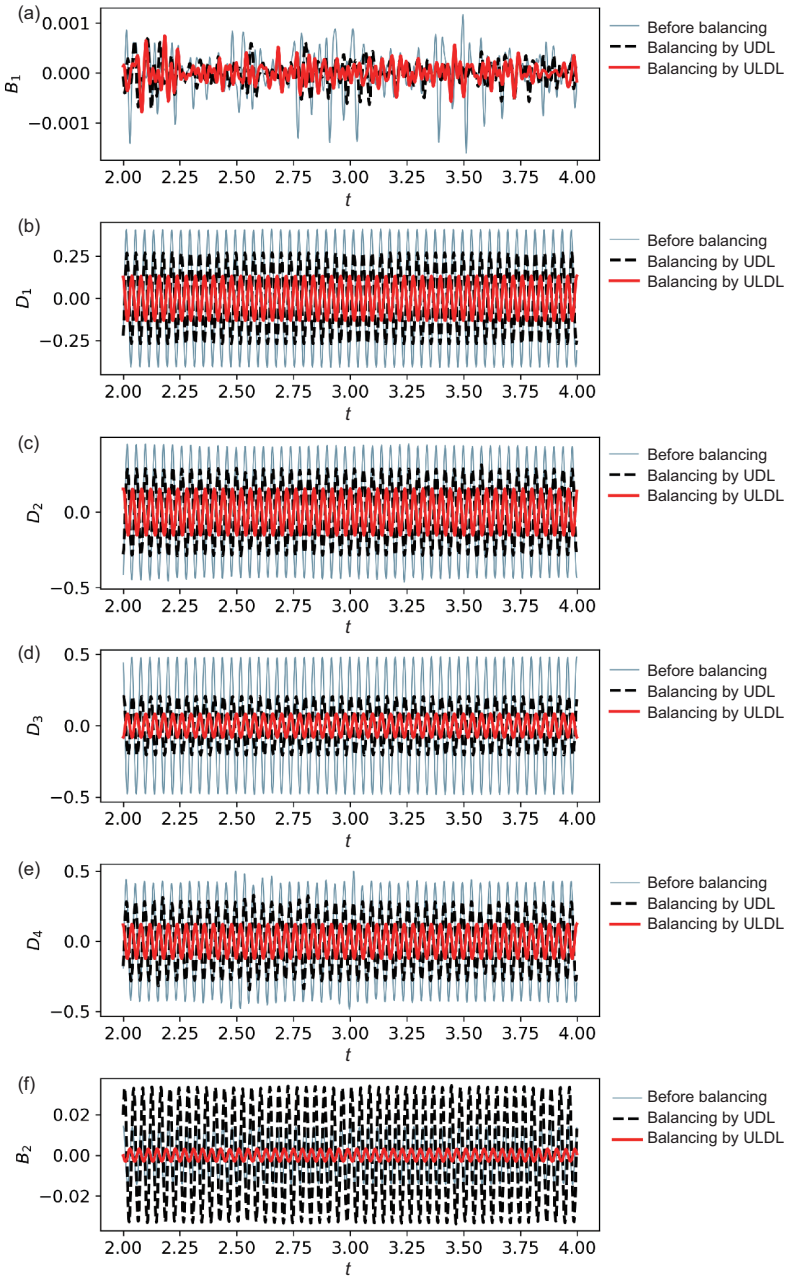

Figure 13 Balancing effects: (a) on node #1, (b) on node #2, (c) on node #3, (d) on node #4, (e) on node #5, (f) on node #6.

information can be involved. All these perspectives deserve further study.

This work was supported by the National Natural Science Foundation of China (Grant Nos. 11972129, 11502161, and 11902184), and National Major Science and Technology Projects of China (Grant No. 2017-IV-0008-0045).

Supporting Information

The supporting information is available online at tech.scichina.com and link.springer.com. The supporting materials are published as submitted, without typesetting or editing. The responsibility for scientific accuracy and content remains entirely with the authors.

1 Yao J, Yang F, Su Y, et al. Balancing optimization of a multiple speeds flexible rotor. J Sound Vib, 2020, 480: 115405
2 Xu J H, Jiao C X, Zou D L, et al. Study on the dynamic behavior of herringbone gear structure of marine propulsion system powered by double-cylinder turbines. Sci China Tech Sci, 2022, 65: 611–630
3 Cao Y, Li F, Cao J, et al. Calibration of a hub dynamic balancing machine based on the least squares method and systematic error analysis. IEEE Access, 2020, 8: 178746
4 Ranjan G, Tiwari R. On-site high-speed balancing of flexible rotor-bearing system using virtual trial unbalances at slow run. Int J Mech Sci, 2020, 183: 105786
5 Zhang S, Zhang Z. Online measuring and estimating methods for the unbalancing vector of thin-disc workpiece based on the adaptive influence coefficient. J Vib Control, 2021, 27: 1753–1764
6 Bishop R E D, Gladwell G M L. The vibration and balancing of an

unbalanced flexible rotor. J Mech Eng Sci, 1959, 1: 66–77
7 Bishop R E D, Parkinson A G. On the use of balancing machines for flexible rotors. J Eng Ind, 1972, 94: 561–572
8 Goodman T P. A least-squares method for computing balance corrections. J Eng Ind, 1964, 86: 273–277
9 Lund J W, Tonnesen J. Analysis and experiments on multi-plane balancing of a flexible rotor. J Eng Ind, 1972, 94: 233–242
10 Zhao S, Ren X, Deng W, et al. A transient characteristic-based balancing method of rotor system without trail weights. Mech Syst Signal Process, 2021, 148: 107117
11 Untaroiu C D, Allaire P E, Foiles W C. Balancing of flexible rotors using convex optimization techniques: Optimum min-max LMI influence coefficient balancing. J Vib Acoust, 2008, 130: 021006
12 Wang X. SQP algorithms in balancing rotating machinery. Mech Syst Signal Process, 2007, 21: 1469–1478
13 Messager T, Pyrz M. Discrete optimization of rigid rotor balancing. J Mech Sci Technol, 2013, 27: 2231–2236
14 Kang Y, Lin T W, Chang Y J, et al. Optimal balancing of flexible rotors by minimizing the condition number of influence coefficients. Mech Mach Theory, 2008, 43: 891–908
15 Li G, Lin Z, Allaire P E. Robust optimal balancing of high-speed machinery using convex optimization. J Vib Acoust, 2008, 130: 031008
16 Zhang Z X, Zhang Q, Li X L, et al. The whole-beat correlation method for the identification of an unbalance response of a dual-rotor system with a slight rotating speed difference. Mech Syst Signal Process, 2011, 25: 1667–1673
17 Zhang Z X, Wang L Z, Jin Z J, et al. Non-whole beat correlation method for the identification of an unbalance response of a dual-rotor system with a slight rotating speed difference. Mech Syst Signal Process, 2013, 39: 452–460
18 Tresser S, Dolev A, Bucher I. Dynamic balancing of super-critical rotating structures using slow-speed data via parametric excitation. J Sound Vib, 2018, 415: 59–77
19 Khulief Y A, Oke W, Mohiuddin M A. Modally tuned influence coefficients for low-speed balancing of flexible rotors. J Vib Acoust, 2014, 136: 024501
20 Deepthikumar M B, Sekhar A S, Srikanthan M R. Modal balancing of flexible rotors with bow and distributed unbalance. J Sound Vib, 2013, 332: 6216–6233
21 Villafane Saldarriaga M, Steffen Jr V, Der Hagopian J, et al. On the balancing of flexible rotating machines by using an inverse problem approach. J Vib Control, 2011, 17: 1021–1033
22 Han D J. Generalized modal balancing for non-isotropic rotor systems. Mech Syst Signal Process, 2007, 21: 2137–2160
23 Li X, Zheng L, Liu Z. Balancing of flexible rotors without trial weights based on finite element modal analysis. J Vib Control, 2013, 19: 461–470
24 Yue C, Ren X, Yang Y, et al. Unbalance identification of speed-variant rotary machinery without phase angle measurement. Shock Vib, 2015, 2015: 934231
25 Li K, Peng C, Deng Z, et al. Field dynamic balancing for active magnetic bearings supporting rigid rotor shaft based on extended state observer. Mech Syst Signal Process, 2021, 158: 107801
26 Zheng S, Wang C. Rotor balancing for magnetically levitated TMPs integrated with vibration self-sensing of magnetic bearings. IEEE ASME Trans Mechatron, 2021, 26: 3031–3039
27 Duan P H, Xie Z J, Kang X D, et al. Self-supervised learning-based oil spill detection of hyperspectral images. Sci China Tech Sci, 2022, 65: 793–801
28 Shen T, Dong Y L, He D X, et al. Online identification of time-varying dynamical systems for industrial robots based on sparse Bayesian learning. Sci China Tech Sci, 2022, 65: 386–395
29 Ting J A, Mistry M N, Peters J, et al. A Bayesian approach to nonlinear parameter identification for rigid body dynamics. In: Robotics: Science and Systems. Philadelphia: University of Pennsylvania, 2006. 32–39
30 Atkeson C G, An C H, Hollerbach J M. Estimation of inertial parameters of manipulator loads and links. Int J Robot Res, 1986, 5: 101–119
31 Haruno M, Wolpert D M, Kawato M. MOSAIC model for sensorimotor learning and control. Neural Comput, 2001, 13: 2201–2220
32 Calinon S, D'halluin F, Sauser E, et al. Learning and reproduction of gestures by imitation. IEEE Robot Automat Mag, 2010, 17: 44–54
33 Ledezma F, Haddadin S. First-order-principles-based constructive network topologies: An application to robot inverse dynamics. In: Proceedings of the 2017 IEEE-RAS 17th International Conference on Humanoid Robotics (Humanoids). Birmingham: IEEE, 2017. 438–445
34 Zhang W, Li X, Ma H, et al. Federated learning for machinery fault diagnosis with dynamic validation and self-supervision. Knowledge-Based Syst, 2021, 213: 106679
35 Zhang W, Li X, Li X. Deep learning-based prognostic approach for lithium-ion batteries with adaptive time-series prediction and on-line validation. Measurement, 2020, 164: 108052
36 Ding B, Wu J, Chuang S, et al. Sparsity-assisted intelligent condition monitoring method for aero-engine main shaft bearing. Trans Nanjing Univ Aeronaut Astronaut, 2020, 37: 508–516
37 Zhao Z, Li T, An B, et al. Model-driven deep unrolling: Towards interpretable deep learning against noise attacks for intelligent fault diagnosis. ISA Trans, 2022, 129: 644–662
38 Lutter M, Listmann K, Peters J. Deep lagrangian networks for end-to-end learning of energy-based control for under-actuated systems. arxiv: 1907.04489
39 Zhong S, Li L, Chen H, et al. A novel balancing method for rotor using unsupervised deep learning. Shock Vib, 2021, 2021: 1800164
40 Chen H, Zhong S, Lu Z, et al. Analysis on multi-mode nonlinear resonance and jump behavior of an asymmetric rolling bearing rotor. Arch Appl Mech, 2021, 91: 2991–3009